Paper II

Free energy diagram for the heterogeneous enzymatic hydrolysis of the glycosidic bonds in cellulose

Trine Holst Sørensen, Nicolaj Cruys-Bagger, Kim Borch & Peter Westh

Trine Holst Sørensen, Nicolaj Cruys-Bagger, Kim Borch and Peter Westh

Access the most updated version of this article at doi: 10.1074/jbc.M115.659656

Find articles, minireviews, Reflections and Classics on similar topics on the JBC Affinity Sites.

Alerts:
- When this article is cited
- When a correction for this article is posted

Click here to choose from all of JBC's e-mail alerts

This article cites 68 references, 16 of which can be accessed free at
http://www.jbc.org/content/290/36/22203.full.html#ref-list-1

Free Energy Diagram for the Heterogeneous Enzymatic Hydrolysis of Glycosidic Bonds in Cellulose*

Trine Holst Sørensen‡, Nicolaj Cruys-Bagger‡, Kim Borch§, and Peter Westh‡1

From ‡Roskilde University, NSM, Research Unit for Functional Biomaterials, 1 Universitetsvej, Building 28, DK-4000 Roskilde, Denmark and §Novozymes A/S, Krogshøjvej 36, DK-2880 Bagsværd, Denmark

Background: Heterogeneous enzyme catalysis is common but has rarely been rationalized through free energy diagrams.
Results: The thermodynamic properties of stable and activated cellulase complexes are reported.
Conclusion: The rate of enzyme-substrate complexation is entropy-controlled, whereas dissociation is controlled by enthalpy.
Significance: Supposedly, this is the first elucidation of the transition states for the complexation and dissociation steps of a cellulase.

Kinetic and thermodynamic data have been analyzed according to transition state theory and a simplified reaction scheme for the enzymatic hydrolysis of insoluble cellulose. For the cellobiohydrolase Cel7A from *Hypocrea jecorina* (*Trichoderma reesei*), we were able to measure or collect relevant values for all stable and activated complexes defined by the reaction scheme and hence propose a free energy diagram for the full heterogeneous process. For other Cel7A enzymes, including variants with and without carbohydrate binding module (CBM), we obtained activation parameters for the association and dissociation of the enzyme-substrate complex. The results showed that the kinetics of enzyme-substrate association (*i.e.* formation of the Michaelis complex) was almost entirely entropy-controlled and that the activation entropy corresponded approximately to the loss of translational and rotational degrees of freedom of the dissolved enzyme. This implied that the transition state occurred early in the path where the enzyme has lost these degrees of freedom but not yet established extensive contact interactions in the binding tunnel. For dissociation, a similar analysis suggested that the transition state was late in the path where most enzyme-substrate contacts were broken. Activation enthalpies revealed that the rate of dissociation was far more temperature-sensitive than the rates of both association and the inner catalytic cycle. Comparisons of one- and two-domain variants showed that the CBM had no influence on the transition state for association but increased the free energy barrier for dissociation. Hence, the CBM appeared to promote the stability of the complex by delaying dissociation rather than accelerating association.

Free energy diagrams are undoubtedly one of the most useful and fundamental ways to illustrate and explain enzyme catalysis, and essentially any biochemistry textbook uses profiles of free energy and reaction coordinates to introduce enzyme func-

tion. However, in the case of enzyme activity at interfaces (*i.e.* heterogeneous enzyme catalysis), free energy diagrams have rarely been used. This may appear surprising in light of the common use of such diagrams within related fields, including catalysis at inorganic interfaces, and further analyses of free energy barriers appear promising in mechanistic studies of interfacial enzyme catalysis, which is common both *in vivo* (1) and in technology (2, 3). In the current work, we present free energy profiles for the enzymatic hydrolysis of cellulose with special emphasis on activation parameters for complexation and dissociation of enzyme and the insoluble substrate. Specifically, we investigated cellobiohydrolases from the glycoside hydrolase family 7. These enzymes utilize the retaining catalytic mechanism, which is similar to that seen in many other glycoside hydrolase families and understood on an atomistic level (4, 5). Cellobiohydrolases have recently attracted particular research interest, which is at least in part driven by their role in different present day challenges, including the distribution of carbon between soil and atmosphere (6, 7) and the utilization lignocellulosic feedstock in sustainable industries (8). Here, we examine the wild-type and some variants of two cellobiohydrolases (both called Cel7A) from *Hypocrea jecorina* and *Rasamsonia emersonii*.

One key element of the aforementioned retaining mechanism is a transient glycosyl enzyme intermediate that is flanked by oxocarbenium ion-like transition states (4), and the properties of these species for the specific case of Cel7A hydrolyzing cellulose have recently been discussed on the basis of different types of molecular modeling (9–14). This theoretical work has provided important information on the structure and processive movement of the cellulose strand in the 5-nm-long binding tunnel, which houses the active site, and suggested (12, 14) that formation of the intermediate (so-called glycosylation) is the rate-limiting step in the catalytic reaction sequence. One study computed a catalytic rate constant around 11 s^{-1} for glycosylation (14), and this is in line with experimental attempts to single out k_{cat} for Cel7A acting on insoluble cellulose (15–18). In most cases, however, the maximal specific rate at quasi-steady state for a monocomponent cellobiohydrolase hydrolyzing insoluble cellulose at room temperature is 1 or 2 orders of magnitude lower than this (16, 19, 20). This was confirmed in the companion article (71), which showed maximal specific

1 To whom correspondence should be addressed. Tel.: 45-4674-2879; Fax: 45-4674-3011; E-mail: pwesth@ruc.dk.

Free Energy Diagram for Cellobiohydrolase Cel7A

rates, $_pV_{max}/E_0$ (subscript p in front of the parameter indicates its relationship to the processive Scheme 1 in the companion article), of about 0.1 s^{-1} at room temperature for the investigated Cel7A enzymes. The divergence between k_{cat} (defined as the turnover of the Michaelis complex in the inner catalytic cycle) and the maximal steady state rate probably relies on the heterogeneous process for Cel7A, which in addition to the catalytic steps that parallel those seen for glycoside hydrolases acting on soluble substrates includes adsorption to and dissociation from the insoluble substrate. Thus, before reaching the Michaelis complex, the enzyme must adsorb to the interface, diffuse laterally to find an attack site, and translocate a sizable piece of the cellulose strand (~10 glucopyranose units) from the crystalline substrate into the binding tunnel. Different arguments have been made that this multifaceted association process or its reversal (dissociation) at the end of a processive run could be much slower than the inner catalytic cycle and hence that the on- or off-rate, rather than the actual catalysis, could be rate-limiting for cellobiohydrolases (16, 20–25). This latter interpretation would reconcile the disparity of k_{cat} and $_pV_{max}/E_0$ simply because the catalytic cycle was a comparably faster step and hence had little influence on the overall reaction rate at quasi-steady state. Unfortunately, molecular details of the association and dissociation steps are not nearly as well understood as the catalytic cycle. This is at least in part because adsorbed species cannot be crystallized and hence structural changes along the adsorption (and desorption) reaction path remain mostly unknown.

To elucidate some aspects of the association and dissociation steps, we combined kinetic and thermodynamic data from the companion article (71), additional measurements reported here, and literature data and analyzed these data along the lines of the transition state theory. Based on this, we have proposed a free energy diagram for the course of the heterogeneous catalysis and estimated enthalpic and entropic contributions to the free energy changes. As indicated above, structural and kinetic information on adsorption and desorption is still too elusive to design and analyze a full heterogeneous reaction scheme composed by elementary reactions (akin to those describing the catalytic cycle (14)). Instead, we used a coarser approach, which merges some putative steps and describes processive catalysis by three composite rate constants and a processivity number (26, 27). Incomplete models such as this have previously proven useful in attempts to assess properties of stable and activated complexes along the reaction path of complicated enzyme reactions (28–30), although exact correlations between free energy and structure obviously cannot be established when elementary steps have been lumped together in composite reactions.

The analysis showed that complexation (formation of the Michaelis complex) and dissociation of Cel7A were limited by comparable free energy barriers but that the balance of entropic and enthalpic contributions was very different for these two steps. This provided some fundamental information on the nature of the transition states, the role of the carbohydrate binding domain (CBM),[2] and the sensitivity to temperature of these two steps.

---

[2] The abbreviations used are: CBM, carbohydrate binding domain; CORE, catalytic domain; PSS, pre-steady state; Hj_{CBM}, cellobiohydrolase Cel7A from *H.*

Experimental Procedures

Enzymes—We used the same cellobiohydrolases as in the companion article (71), and procedures regarding cloning, expression, purification, and concentration determination are described there. The enzymes were Cel7A wild types from, respectively, *R. emersonii* (*Re*) and *H. jecorina* (*Hj*) (often identified by the name of its anamorph, *Trichoderma reesei*). The latter is a two-domain enzyme with a catalytic domain (CORE) module and a CBM, whereas the former has a one-domain architecture with no CBM. We also investigated a one-domain variant of the *Hj* enzyme without linker and CBM and a chimera composed of the *Re* enzyme and the linker and CBM from *Hj* Cel7A. In the following, we will use the same abbreviations as in the companion article (71) for these four enzymes, *i.e.* Hj_{CBM}, Re_{CORE}, Hj_{CORE}, and Re_{CBM}, respectively.

Product Profile—To estimate processivity, we measured the concentrations of products generated by the four enzymes at temperatures from 10 to 50 °C (*i.e.* the same temperature range used for the kinetic measurements in the companion article (71)). The reactions were started by the addition of 80 μl of enzyme stock solution to 920 μl of preheated or -cooled Avicel solution in 2-ml Eppendorf tubes. The final enzyme concentration was 0.40 μM as in the kinetic experiments in the companion article (71). All samples were incubated for 1 h with orbital shaking at 1100 rpm and subsequently quenched by 100 μl of 1.0 M NaOH. Following centrifugation for 3 min at 3500 rpm at 5 °C (Hereaus Multifuge 3 S-R), the concentrations of glucose, cellobiose, and cellotriose in the supernatants were quantified in a Dionex ICS-5000 ion chromatograph (Thermo Fisher Scientific, Waltham, MA). Details of the chromatographic procedure have been described previously (31). A blank (without enzyme) was included and subtracted for all measurements.

Pre-steady State Kinetics—To elucidate the temperature dependence of the catalytic rate constant, $_pk_{cat}$, we investigated the pre-steady state kinetics of Hj_{CBM} on Avicel (the same substrate as in the companion article (71)). We measured the production of cellobiose in real time with an amperometric biosensor functionalized with the oxidoreductase cellobiose dehydrogenase from *Phanerochaete chrysosporium* (32) and analyzed the results as described previously (15, 27). We used the experimental temperatures 5, 25, and 50 °C, and the enzyme concentration was 150 nM. Duplicate measurements were performed with 5–10 different Avicel loads between 0.5 and 5 g/liter at the three temperatures.

Results

The aim of this work was to elucidate changes in free energy, enthalpy, and entropy of stable and activated complexes along a previously suggested reaction path for processive cellulases (26, 27). For the current use, we made the additional assumption that consecutive processive steps will be thermodynamically similar, and we hence only include one catalytic step in the diagram. This means that the reaction sequence we want to describe may be written as shown in Scheme 1.

---

jecorina (wild type with CORE and CBM); Hj_{CORE}, *H. jecorina* Cel7A variant without CBM; Re_{CORE}, Cel7A from *R. emersonii* (wild type without CBM); Re_{CBM}, chimeric enzyme with CORE from *R. emersonii* and CBM from *H. jecorina*.

$$E + C_m \xrightarrow{\ _pk_{on}\ } EC_m \xrightarrow{\ _pk_{cat}\ } EC_{m-1} + C \xrightarrow{\ _pk_{off}\ } E + C_{m-1} + C$$
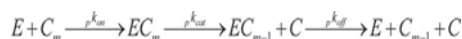
SCHEME 1. Reaction path underlying the analysis. EC_m and EC_{m-1} are interpreted as the Michaelis complexes of enzyme and a cellulose strand of either m or $m-1$ cellobiose units. E and C represent free enzyme and cellobiose, respectively (see the companion article (71) for more details).
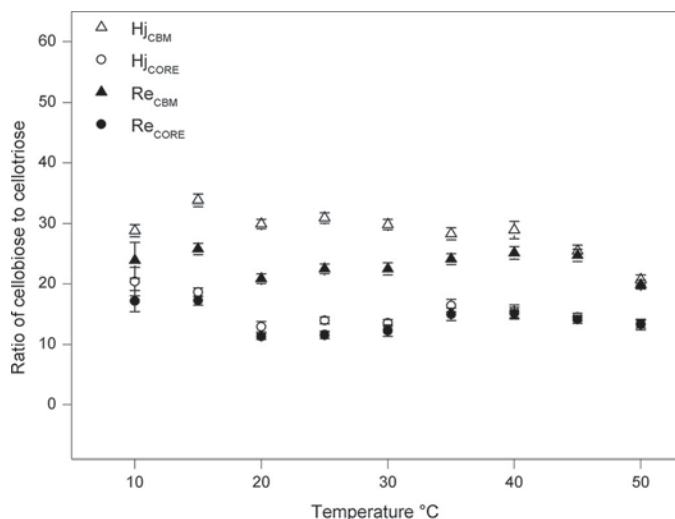

FIGURE 1. **Processivity estimated as the product ratio, $n_p \sim$ [cellobiose]/[cellotriose].** The concentrations were measured by ion chromatography after 1-h hydrolysis trials. *Triangles* identify enzymes with a CBM, and *circles* are for one-domain variants. *Open* and *closed symbols* signify enzymes from *H. jecorina* and *R. emersonii*, respectively.

All three steps in Scheme 1 are composite reactions that lump together different putative elementary steps. Thus, the complexation governed by $_pk_{on}$ includes adsorption to the surface, threading, and formation of the Michaelis complex, EC_m. The catalytic step incorporates the hydrolytic reaction sequence (14) followed by one processive step and release of the product so that a new Michaelis complex with a slightly shortened strand, EC_{m-1}, is formed. Finally, dissociation includes dethreading of the binding tunnel and release from the surface. To appraise free energy, enthalpy, and entropy of activated and stable complexes along this path, we need values of the three rate constants and their temperature dependence together with (equilibrium) thermodynamic functions for enzyme-substrate association and hydrolysis of a glycosidic bond in cellulose. This makes up a total of 15 parameters (standard changes in free energy, enthalpy, and entropy for three transition states and two equilibria). In the next sections we collect this information from current experiments, the companion article (71), and earlier literature.

Association and Dissociation—Rate constants for these steps can be derived from the kinetic parameters in the companion article (71) provided that the processivity number, n, is known. Many studies have suggested that n can be approximated from the relative concentrations of soluble products, although controversies remain regarding the exact interpretation of such data (33–36). We used the simplest approach, and estimated n as the ratio [cellobiose]/[cellotriose] obtained from the chromatographic measurements. Results in Fig. 1 show n values calculated in this way in 5 °C increments between 10 and 50 °C for all investigated enzymes. The value for Hj_{CBM} around room temperature ($n \sim 30$) is in line with earlier estimates based on
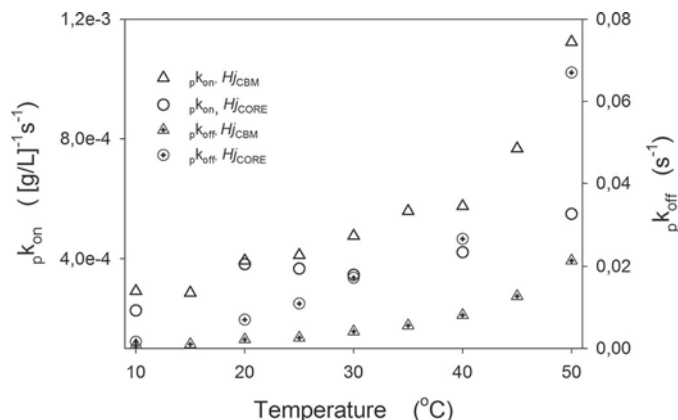
Free Energy Diagram for Cellobiohydrolase Cel7A

FIGURE 2. **Temperature dependence of the rate constants $_pk_{on}$ (*left ordinate*) and $_pk_{off}$ (*right ordinate*) calculated from Equations 1 and 2 using data from the companion article (71).** *Triangles* identify enzymes with a CBM, and *circles* are for one-domain variants.

either product ratios or other experimental approaches (20, 23, 35, 37, 38). The two main results in Fig. 1 are that variants with a CBM have moderately higher processivity that their one-domain analogs and that the processivity shows little dependence on temperature. We are only aware of one earlier study on the temperature dependence of n for cellulases, and in this case, Kostylev *et al.* (39) found a similar (limited) effect of temperature for the exocellulase Cel48A from *Thermobifida fusca*.

The main purpose of measuring processivities in the current context is that they provide a way to calculate the rate constants $_pk_{on}$ and $_pk_{off}$ from the kinetic parameters $_pV_{max}/E_0$ and $_p\eta$. Thus, if $_pk_{cat} \gg {}_pk_{off}$, we may write the following equations (26).

$$k_{on} = \frac{_p\eta}{n_p} \qquad \text{(Eq. 1)}$$

$$k_{off} = \frac{_pV_{max}}{E_0 n_p} \qquad \text{(Eq. 2)}$$

In Equations 1 and 2, $_p\eta$ and $_pV_{max}/E_0$ are, respectively, the specificity constant and the maximal specific rate, which are both listed between 10 and 50 °C in Table 1 of the companion article (71). The underlying assumption that $_pk_{cat} \gg {}_pk_{off}$ has previously been confirmed at room temperature where $_pk_{cat}$ was 2–3 orders of magnitude larger (16, 19), and as we will see below, it also appears reasonable at the somewhat higher temperatures studied here. Examples of rate constants calculated in this way are plotted as a function of temperature in Fig. 2.

The rate constants shown in Fig. 2 and the analogous values for the *R. emersonii* enzymes were used to estimate the transition state free energy g for association and dissociation, respectively. Specifically, we inserted relevant rate constants into the Eyring equation (40).

$$\Delta G^{\neq} = -RT \ln\left[\frac{h_p k_i}{k_B T}\right] \qquad \text{(Eq. 3)}$$

where h and k_B are Planck's and Boltzmann's constants, respectively; $_pk_i$ is the rate constant (either $_pk_{on}$ or $_pk_{off}$); R is the gas constant, and T is temperature. We note that the identification

≋ASBMB

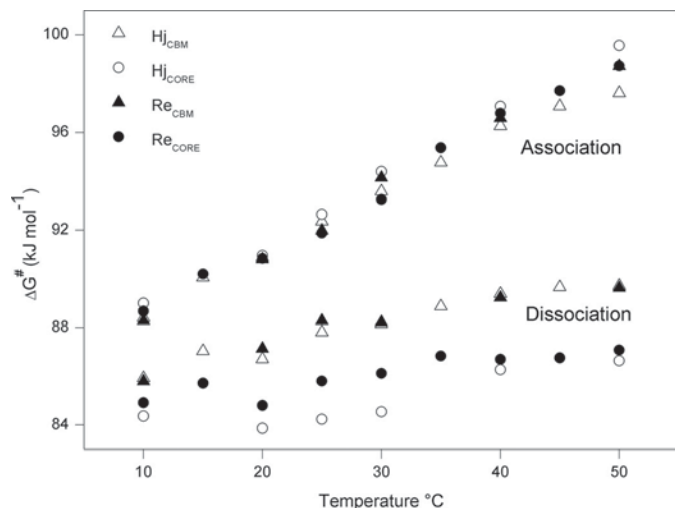## Free Energy Diagram for Cellobiohydrolase Cel7A

FIGURE 3. **Transition state free energies determined from Equation 3 and plotted as a function of temperature for both one-domain (*circles*) and two-domain (*triangles*) variants of Cel7A from *H. jecorina* (*open symbols*) and *R. emersonii* (*filled symbols*).**

FIGURE 4. **Eyring plots for association (calculated from $_pk_{on}$) and dissociation (calculated from $_pk_{off}$) for the four investigated enzymes.** *Triangles* represent two-domain enzymes (*i.e.* with a CBM), and *circles* are for one-domain enzymes. The slope, α, specifies the activation enthalpy, $\alpha = -\Delta H^{\neq}/R$.

of a transition state in a diffusion-controlled association process is outside the original scope of the theory. However, it has been argued that transition state theory may be applied to protein-protein association in solution (41, 42), and in the current work, we used a similar approach for the adsorption on the substrate. Equation 3 is the simplified form of the Eyring equation, which assumes that the transmission coefficient, κ, is 1, and this means that the extrathermodynamic contribution to the activation free energy, $\Delta G_{extra} = -RT \ln \kappa$, is neglected. It appears from Equations 1 and 2 that both $_pk_{on}$ and $_pk_{off}$ are inversely proportional to n, and these rate constants (Fig. 2) are therefore sensitive to possible systematic errors in the processivity measurements, which were mentioned above. However, the logarithmic conversion to $\Delta G^{\neq}$ in Equation 3 tends to dampen the effect of this, and even if the processivity number was wrong by as much as a factor of 2, it would only change $\Delta G^{\neq}$ by about 1.7 kJ/mol. As comparisons of current n values and earlier measurements (see above) suggested quite good accordance, imprecise n values do not appear to be a major cause of error on the activation parameters. Transition state free energies calculated under the assumption that $\Delta G_{extra} = 0$ (sometimes called phenomenological activation free energies (43)) for association ($\Delta G_{assoc}^{\neq}$) and dissociation ($\Delta G_{dissoc}^{\neq}$) are plotted as a function of temperature for each of the four investigated enzymes in Fig. 3.

The results in Fig. 3 show that the CBM had no effect on $\Delta G_{assoc}^{\neq}$. Specifically, the average difference in $\Delta G_{assoc}^{\neq}$ between one- and two-domain enzymes at the same temperature was 0.3 ± 0.7 kJ/mol. Similarly, we did not detect significant differences in $\Delta G_{assoc}^{\neq}$ when comparing enzymes from *H. jecorina* and *R. emersonii* (all association data in Fig. 3 overlap). It follows that neither the CBM nor natural adaptation to higher temperatures appeared to affect the free energy barrier of association in this study. For dissociation, however, we found a small but significant increase in activation free energy for enzymes with CBM ($\Delta G_{dissoc}^{\neq}$ was 2.6 ± 0.8 kJ/mol higher on average for two-domain enzymes in Fig. 3). The most conspic-
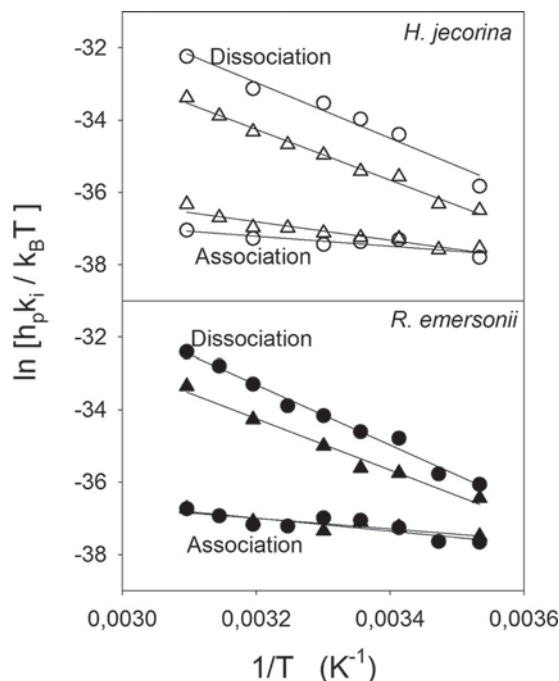
uous result in Fig. 3 was a much stronger temperature dependence of $\Delta G_{assoc}^{\neq}$ compared with $\Delta G_{dissoc}^{\neq}$. To further elucidate this, we plotted $\ln(h_p k_i/k_B T)$ against $1/T$ in Fig. 4. This is a so-called Eyring plot, which has a slope of $-\Delta H^{\neq}/R$ where $\Delta H^{\neq}$ is the activation enthalpy as defined in transition state theory. It appears that the (linear) Eyring plots in Fig. 4 were much steeper for dissociation compared with association. The shallow slope for association meant that that $\Delta H_{assoc}^{\neq}$ was very low (15–20 kJ/mol) with no distinctive differences between the four investigated enzymes. This similarity between the different enzyme variants suggested that the CBM did not affect the enthalpy of the transition state for the association step. For the dissociation process, the transition state enthalpies were much higher with $\Delta H_{dissoc}^{\neq}$ values between 60 and 70 kJ/mol. In this case, a moderate effect of the CBM could be singled out because $\Delta H_{dissoc}^{\neq}$ for enzymes with a CBM was 5–10 kJ/mol higher than for the corresponding one-domain enzymes. Based on the above estimates of, respectively, free energies and enthalpies of activation, the entropic contributions $T\Delta S_{assoc}^{\neq} = \Delta H_{assoc}^{\neq} - \Delta G_{assoc}^{\neq}$ and $T\Delta S_{dissoc}^{\neq} = \Delta H_{dissoc}^{\neq} - \Delta G_{dissoc}^{\neq}$ were calculated. These results consistently showed that this entropic contribution was large and negative (-70 to -80 kJ/mol) for association and quite small (-20 to -25 kJ/mol) for dissociation.

Catalysis—Previous work has suggested that the catalytic rate constant for Cel7A acting on insoluble substrate is 5–10 s^{-1} around room temperature (14–18). Surprisingly, the temperature dependence of this parameter has not been reported previously for processive cellulases. Many studies have investigated the temperature dependence of the hydrolytic rate, but as argued above, the actual catalysis is unlikely to be rate-limiting under most conditions, and it follows that changes in the observed overall rate do not necessarily provide any insight into
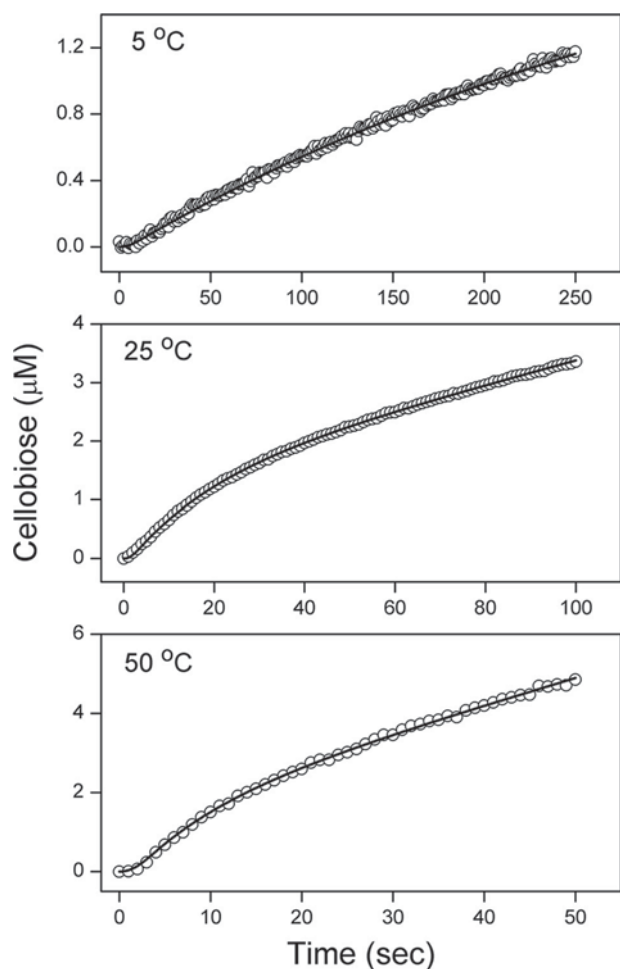
FIGURE 5. **Examples of progress curves for Hj_{CBM} hydrolyzing Avicel at different temperatures.** The *points* are raw data from biosensor measurements, and the *lines* are best fits of a kinetic model describing processive cellulases (see "Results" for details). The initial, sigmoidal part of the curves (*e.g.* the first ~30 s at 25 °C) is the so-called burst phase, and the subsequent, near-linear course reflects quasi-steady state. The enzyme concentration was 150 nM, and the Avicel load was 3.0 g/liter at 5 °C and 5.0 g/liter at 25 and 50 °C.

the magnitude of $_pk_{cat}$. One way to quantify rate constants for the faster (*i.e.* not rate-determining) steps in an enzyme reaction is pre-steady state (PSS) kinetic measurements. Examples of PSS measurements for Hj_{CBM} at 5, 25, and 50 °C are shown in Fig. 5. The *points* represent the raw data (concentration of cellobiose *versus* time), and the *lines* are best fits of a processive kinetic model (27). The first, sigmoidal part of the curves reflects the so-called burst in the PSS regime, whereas the subsequent, near-linear course is interpreted as a quasi-steady state condition (15). It is interesting to note that the duration of the PSS regime for this heterogeneous process is much longer than typically found for enzymes acting on soluble substrates. Thus, the room temperature data in Fig. 5 reaches quasi-steady state within about a 0.5 min, whereas the typical duration of PSS for homogenous enzyme catalysis is in the tens or hundreds of milliseconds (44). The results in Fig. 5 show that the model accounted satisfactorily for the measurements, and the regression analysis of all data (*i.e.* duplicate runs at different substrate loads) showed that $_pk_{cat}$ at 25 °C was 5.3 ± 0.9 s^{-1} in accord with the earlier investigations mentioned above. At 5 and 50 °C

we found $_pk_{cat}$ values of 1.6 ± 0.2 and 10.2 ± 2.1 s^{-1}, respectively. Independent regressions were conducted for duplicate measurements at 5–10 different substrate loads, and the stated $_pk_{cat}$ values are averages and standard deviations for all regressions at a given temperature. We have previously analyzed correlation coefficients for this type of regression for room temperature data (15, 16) and found a moderate mutual interdependence of $_pk_{cat}$ and $_pk_{on}$. This correlation became worse at higher temperature, and this was a main cause of the larger standard deviation at 50 °C. Insertion of $_pk_{cat}$ values in Equation 3 showed that the free energy of activation for the catalytic step, $\Delta G^{\neq}_{cat}$, increased linearly from 67 ± 0.6 kJ/mol at 5 °C to 73 ± 0.8 kJ/mol at 50 °C. An Eyring plot of the catalytic rate constants (not shown) was near linear ($R^2 = 0.97$) and gave an activation enthalpy, $\Delta H^{\neq}_{cat}$, of 29 ± 5 kJ/mol, and the entropic contribution at room temperature, $T\Delta S^{\neq}_{cat} = \Delta H^{\neq}_{cat} - \Delta G^{\neq}_{cat}$, was therefore about −40 kJ/mol.

Thermodynamic Data—Thermodynamic information on adsorption and hydrolysis is also required for the diagram (see Fig. 6). The net affinity of Cel7A for insoluble cellulose has been investigated in several earlier studies. Most recently, Jalak and Väljamäe (45) suggested a multimode binding of Cel7A to crystalline cellulose and reported dissociation constants, K_d, of 3 and 400 nM, respectively, for two binding modes, which showed complete or partial substrate occupancy of the active tunnel. Other studies using a two-site Langmuir model have found dissociation constants in the 10–200 nM range for the high affinity site (18, 46–48), and the affinity of long cellooligosaccharides for a catalytically deficient variant of Cel7A was also in this range (49). Hence, the best estimate for a dissociation constant of the Michaelis complex for Cel7A appears to be in the low to mid nM range. Using $\Delta G^0_{assoc} = -RT \ln(1/K_d)$, this translates into a standard free energy changes of association, ΔG^0_{assoc}, of −40 to −45 kJ/mol. The enthalpy change for the association process, ΔH^0_{assoc}, can be estimated by a Van't Hoff analysis (*i.e.* plots of $\ln(K(T))$ *versus* $1/T$) using either $_pK_m$ or K_p, which are reported in the companion article (71). This approach suggested ΔH^0_{assoc} values of −40 to −50 kJ/mol, and a similar value was found by direct (calorimetric) measurements of ΔH for the binding of cellooctaose to *H. jecorina* Cel7A around room temperature (49). As the values of ΔG^0_{assoc} and ΔH^0_{assoc} are comparable in size, the entropic contribution to association, $T\Delta S^0_{assoc} = \Delta H^0_{assoc} - \Delta G^0_{assoc}$, at room temperature must be close to zero. The last process we need to consider is the hydrolysis of the glycosidic bond. The enthalpy change for the hydrolysis of glycosidic bonds in Avicel is weakly exothermic with a ΔH_{hydrol} of about −4 kJ/mol (50). We are not aware of any experimental data on the standard free energy change, ΔG^0_{hydrol}, for the conversion of Avicel (or any other type of cellulose) into cellobiose. Goldberg and co-workers (51) found that ΔG^0_{hydrol} for the β-1,4-glycosidic bond in cellobiose was about −16 kJ/mol at room temperature and further reported that the free energy change per hydrolyzed glucosidic bond was in general quite constant in longer oligosaccharides. Based on this, we use $\Delta G^0_{hydrol} = -16$ kJ/mol in the diagram below. The lack of direct measurements of this parameter obviously puts some provisos on the interpretation of this step, but we note
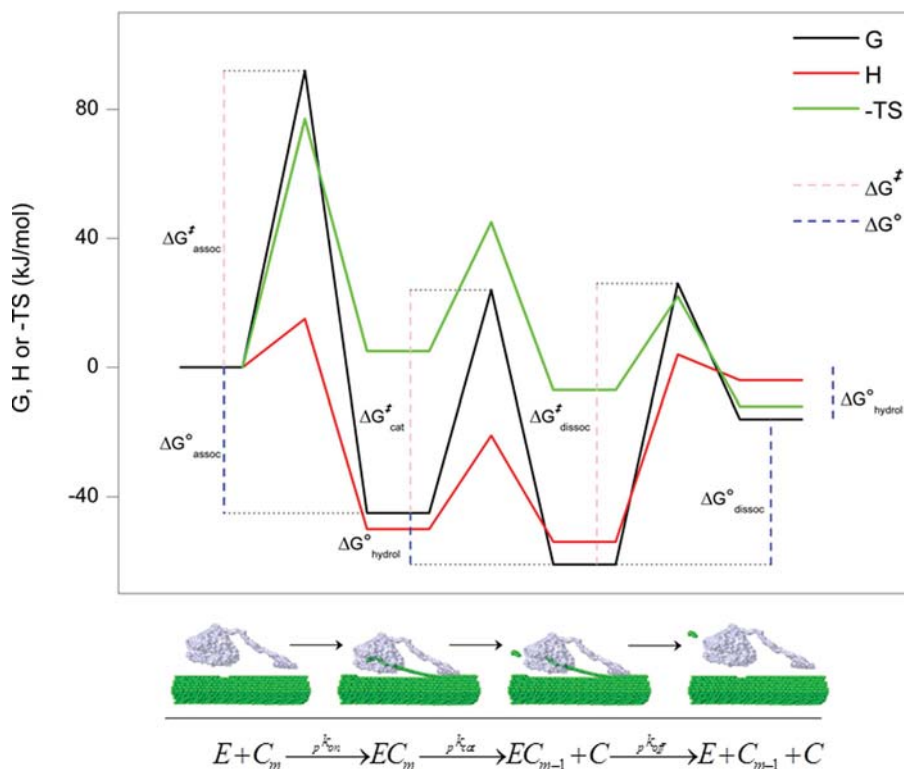
FIGURE 6. **Energy diagram for Cel7A hydrolysis of a glycosidic bond in insoluble cellulose.** The *abscissa* is the reaction path as discussed in the main text and illustrated by the schematics and equations below the figure. The *ordinate* shows changes in free energy (*G*; *black* curve), enthalpy (*H*; *red* curve), and entropy (−*TS*; *green* curve) along the reaction path. Note that the entropic contribution is given as its negative value, −*T*Δ*S*. The diagram defines a total of five changes (three activated complexes and two equilibria), and the thermodynamic functions pertaining to each of these steps are specified by a set of *super-* and *subscript*. For the *G* function, these five steps are identified by the *dashed lines* in the figure, and the *super-* and *subscripts* are given in the associated *symbols*. The same set of *super-* and *subscripts* are used for the *H* and −*TS* functions in the text.

that the value of $\Delta G^0_{\text{hydrol}}$ would have to be very different before it would affect any of the interpretations.

Discussion

For the wild type Hj_{CBM}, we now have room temperature estimates of 15 parameters characterizing stable and activated complexes defined by Scheme 1, and this is illustrated in the diagram in Fig. 6. For the other enzymes, Re_{CORE}, Re_{CBM}, and Hj_{CORE}, we have data for association and dissociation (but not catalysis), and we will return to a comparative discussion of this below. First, we discuss some aspects of the diagram for Hj_{CBM}.

Association—The Michaelis complex (EC_m) has almost the same entropy but a much lower enthalpy than the free enzyme and substrate ($E + C_m$), and enthalpy is hence the main driving force for association around room temperature (Fig. 6). Kinetically, association is governed by a sizable activation free energy ($\Delta G^{\neq}_{\text{assoc}} \sim 92$ kJ/mol), which is dominated by the entropic contribution ($-T\Delta S^{\neq}_{\text{assoc}} \sim 77$ kJ/mol; note that to facilitate visual comparisons of enthalpic and entropic contributions in Fig. 6, the latter are given as their negative values, −*T*Δ*S*). Interestingly, estimates based on the principles proposed in the seminal study by of Page and Jencks (52) suggest that this $-T\Delta S^{\neq}_{\text{assoc}}$ value is comparable with the entropic penalty associated with losses of rotational and translational degrees of freedom of the enzyme. The exact entropic cost of freezing out these degrees of freedom has been debated subsequently (53–56), but most values fall in this range. This coincidence suggests that the transition state is located early in the path of complexation where the

associated enzyme has lost these degrees of freedom but not yet established extensive contacts with the cellulose strand in the binding tunnel. These contacts are associated with comprehensive hydrogen bonding (14, 57, 58) and dehydration of hydrophobic surfaces (49), which will tend to lower both the enthalpic (*red* trace) and entropic (*green* trace) contributions in Fig. 6. We suggest that these contacts are established later in the path of association as the strand moves forward and gradually fills the binding tunnel and thus brings the enthalpy to a large negative value and −*T*Δ*S* back to approximately zero (Fig. 6). The interpretation of a transition state early in the path of association is also in accord with the low activation enthalpy, $\Delta H^{\neq}_{\text{assoc}}$, as little rearrangement of hydrogen bonding (and other interactions) has occurred at this stage. A probable structural interpretation could be that the transition state of association is the initial threading where the end of the cellulose strand must be dislodged from the crystal and moved into the mouth of the binding tunnel. Previous work also supports the notion that early complexes in the association path could be rather unstable. Thus, the work required to abstract a glucopyranose unit from crystalline cellulose is quite high (5–14 kJ/mol depending on position and crystal structure), whereas the affinity in the first part of the catalytic tunnel only contributes −3 to −7 kJ/mol per glucopyranose unit to the standard free energy of binding (49, 59). These numbers underscore that contact interactions in the binding tunnel are unlikely to compensate for the sizable loss in translational entropy until late in the association

path where the strongly interacting subsites near the exit of the tunnel (49, 57, 60) become filled. One interesting aspect of an early transition state governed by entropy is that $_pk_{on}$ is expected to be quite insensitive to interactions in the tunnel (as most of these interactions are established during the downhill part of the free energy trace subsequent to the transition state). As a result, protein engineering that modifies such interactions is predicted to exert only moderate changes of $_pk_{on}$. This prediction was confirmed in a recent study of a Cel7A mutant where a tryptophan in the middle of the tunnel had been replaced by alanine. This enzyme variant showed a markedly reduced affinity for the substrate, but the reduction was almost entirely due to a faster rate of dissociation, whereas $_pk_{on}$ only decreased only about 27% (61).

Catalysis—The free energy barrier for catalysis was about 69 kJ/mol at room temperature, and this is in good accordance with theoretical studies, which have found $\Delta G^{\neq}_{cat}$ values of 65 and 73 kJ/mol (12, 14). The entropic contribution was dominating ($-T\Delta S^{\neq}_{cat} = 40$ kJ/mol), although $\Delta H^{\neq}_{cat}$ was only moderately smaller (29 kJ/mol). Unlike for association and dissociation, the free energy landscape for the inner catalytic cycle of Cel7A has been extensively studied on an atomistic level (9–14). Comparisons of these results and the current observation of a dominant entropic contribution may hint that fixation of the Glu-212 side chain and strain in the substrate chain around subsite −1 could be important destabilizing effects in the transition state. However, proper complementation of the comprehensive theoretical work on catalysis awaits more sophisticated experimental approaches such as measurements of kinetic isotope effects or linear free energy relationships (62–65).

Dissociation—The free energy barrier of dissociation, $\Delta G^{\neq}_{dissoc} \sim 87$ kJ/mol, was comparable with the barrier of association, but in sharp contrast to association, it was dominated by the enthalpic contribution, $\Delta H^{\neq}_{dissoc} \sim 58$ kJ/mol. This together with the observation that the enthalpy of the transition state for dissociation (last maximum in the *red* trace in Fig. 6) was on the same level as the dissociated components suggests that the transition state is located late in the dissociation path with few remaining enzyme-substrate contacts. One direct consequence of the comparably high $\Delta H^{\neq}_{dissoc}$ is that dissociation is accelerated much more by increasing temperatures than the two other steps. To illustrate this, we calculated activation energies, $E_a = \Delta H^{\neq} + RT$, and inserted the results in the Arrhenius equation. This showed that changing from room temperature (where many activity studies are conducted) to the more industrially relevant 50 °C increases the rate constants for association ($_pk_{on}$), catalysis ($_pk_{cat}$), and dissociation ($_pk_{off}$) by factors of 1.7, 2.6, and 6.7, respectively. This strong preferential activation of dissociation may lead to unexpected kinetic changes when the temperature is raised, and some aspects of this were discussed in the companion article (71). Preferential temperature activation of dissociation has also been observed for a β-glucosidase acting on soluble substrate, and in this case, it led to a change in the rate-determining step around 20 °C (66). Below this temperature, dissociation of the enzyme-substrate complex was rate-limiting, but at higher temperatures, formation of the complex became the bottleneck. This parallels

the rapid growth in the dissociation rate found here, although we did not see evidence of a change in the rate-limiting step. The late location of the transition state for dissociation implies that most enzyme-substrate contacts must be broken to reach it, and it follows that $_pk_{off}$ is predicted to depend strongly on these interaction. This is in contrast to the entropy-controlled $_pk_{on}$ (discussed above), which was suggested to be less dependent on the extent of substrate contact. This predicted behavior of $_pk_{on}$ and $_pk_{off}$ was confirmed both in comparisons of enzymes with and without CBM in the current work and in an earlier study of a mutant with weakened substrate interactions in the binding tunnel (61). In both cases, deletion of substrate interactions led to a distinctive rise in $_pk_{off}$ and little or no change in $_pk_{on}$. This suggests that $_pk_{off}$ may be tuned in a controlled way through engineering of targets such as the binding tunnel, loops, CBM, or linker glycans, which have recently also been shown to play a role in substrate interactions (67). This contribution from glycans to substrate interactions also points toward relevance of the organism used in heterologous expression. Thus, variation in the glycosylation pattern of Cel7 enzymes expressed in different organisms has previously been shown to exert a marked effect on enzyme efficiency (68, 69), and this could potentially rely on interactions that reduce $_pk_{off}$.

Comparative Analysis of Different Enzymes—The data in Figs. 2 and 3 provide activation parameters for association and dissociation for all four enzymes, Hj_{CBM}, Re_{CORE}, Hj_{CORE}, and Re_{CBM}, and comparative analysis of this appears to be of interest particularly regarding possible roles of the CBM. For association, the results showed that the binding module did not change any of the measured activation parameters. This strongly suggests that the transition state of association was unaffected by CBM-cellulose interactions. For dissociation, however, we found that the CBM increased the free energy barrier by 3–4 kJ/mol (Fig. 2) and that this difference was due to an increased enthalpic contribution (Fig. 3). This reflects that $_pk_{off}$, but not $_pk_{on}$, was affected by the CBM, and as the stability constant of the enzyme-substrate complex is the ratio of the on- and off-rate constants, these observations showed that the well known increment in substrate affinity generated by the CBM (48, 70) is the result of slower dissociation, whereas the rate of association remained mostly unaffected by the CBM. The difference in the standard free energy of association (ΔG^0_{assoc}) for one- and two-domain enzymes derived from the current data was about 4 kJ/mol, and this affinity contribution of the CBM corresponds to earlier reports (48, 61).

Conclusions—We have used kinetic and thermodynamic data to construct a free energy diagram for the hydrolysis of a β-1,4-glycosidic bond in insoluble cellulose and assessed enthalpic and entropic contributions to the activation free energies. The diagram was based on a reaction scheme that separates the complex heterogeneous process into three basic steps: association, catalysis, and dissociation. This type of simplification is currently necessitated by limitations in both structural and quantitative experimental data for association and dissociation. Rate-limiting steps were only assessed on an empirical level by simple comparisons of rates under typical conditions. This suggested that around room temperature the bottleneck was dissociation, but as this step was accelerated much more by tem-

perature than the others, the importance of dissociation for the overall rate lessened at higher temperatures (see the companion article (71)). Despite the limitations associated with an incomplete model picture, it was possible to elucidate different mechanistic aspects. We found that the kinetics of forming the Michaelis complex was primarily governed by large, unfavorable entropy of the transition state. The enthalpy of this transition state was only slightly increased compared with the unbound enzyme and substrate, and this balance of a high entropy but low enthalpy activation barrier has previously been found for a processive chitinase acting on insoluble substrate (25). This distribution of the enthalpic and entropic contributions to $\Delta G^{\neq}$ meant that the on-rate only increased slowly with temperature, and on a structural level, it suggested that the transition state occurred early in the path of the association where the enzyme has lost rotational and translational degrees of freedom but not yet established extensive interactions in the binding tunnel. For dissociation, the enthalpic contribution to the activation free energy was dominant, and this suggested that the transition state for this step was also close to the free forms, *i.e.* late in the dissociation path at a stage where most enzyme-substrate interactions had been broken. This high activation enthalpy also meant that the rate of dissociation increased much more with temperature than the rate of the two preceding steps. The CBM had no detectable effect on the activation parameters for association, but it increased the free energy barrier of dissociation. This meant that the higher affinity brought about by the CBM relies on a delay of dissociation rather than an increased rate of association.

References

1. Gelb, M. H., Min, J. H., and Jain, M. K. (2000) Do membrane-bound enzymes access their substrates from the membrane or aqueous phase: interfacial versus non-interfacial enzymes. *Biochim. Biophys. Acta* **1488,** 20–27
2. Illanes, A., Wilson, L., and Vera, C. (2013) *Problem Solving in Enzyme Biocatalysis*, John Wiley and Sons, Chichester, UK
3. Kirk, O., Borchert, T. V., and Fuglsang, C. C. (2002) Industrial enzyme applications. *Curr. Opin. Biotechnol.* **13,** 345–351
4. Vocadlo, D. J., and Davies, G. J. (2008) Mechanistic insights into glycosidase chemistry. *Curr. Opin. Chem. Biol.* **12,** 539–555
5. Withers, S. G. (2001) Mechanisms of glycosyl transferases and hydrolases. *Carbohydr. Polym.* **44,** 325–337
6. Davidson, E. A., and Janssens, I. A. (2006) Temperature sensitivity of soil carbon decomposition and feedbacks to climate change. *Nature* **440,** 165–173
7. German, D. P., Marcelo, K. R. B., Stone, M. M., and Allison, S. D. (2012) The Michaelis-Menten kinetics of soil extracellular enzymes in response to temperature: a cross-latitudinal study. *Glob. Chang. Biol.* **18,** 1468–1479
8. Wilson, D. B. (2009) Cellulases and biofuels. *Curr. Opin. Biotechnol.* **20,** 295–299
9. Li, J., Du, L., and Wang, L. (2010) Glycosidic-bond hydrolysis mechanism catalyzed by cellulase Cel7A from *Trichoderma reesei*: a comprehensive theoretical study by performing MD, QM, and QM/MM calculations. *J. Phys. Chem. B* **114,** 15261–15268
10. Yan, S., Li, T., and Yao, L. (2011) Mutational effects on the catalytic mechanism of cellobiohydrolase I from *Trichoderma reesei. J. Phys. Chem. B* **115,** 4982–4989
11. Barnett, C. B., Wilkinson, K. A., and Naidoo, K. J. (2010) Pyranose ring transition state is derived from cellobiohydrolase I induced conformational stability and glycosidic bond polarization. *J. Am. Chem. Soc.* **132,** 12800–12803
12. Barnett, C. B., Wilkinson, K. A., and Naidoo, K. J. (2011) Molecular details from computational reaction dynamics for the cellobiohydrolase I glycosylation reaction. *J. Am. Chem. Soc.* **133,** 19474–19482
13. Knott, B. C., Crowley, M. F., Himmel, M. E., Ståhlberg, J., and Beckham, G. T. (2014) Carbohydrate-protein interactions that drive processive polysaccharide translocation in enzymes revealed from a computational study of cellobiohydrolase processivity. *J. Am. Chem. Soc.* **136,** 8810–8819
14. Knott, B. C., Haddad Momeni, M., Crowley, M. F., Mackenzie, L. F., Götz, A. W., Sandgren, M., Withers, S. G., Ståhlberg, J., and Beckham, G. T. (2014) The mechanism of cellulose hydrolysis by a two-step, retaining cellobiohydrolase elucidated by structural and transition path sampling studies. *J. Am. Chem. Soc.* **136,** 321–329
15. Cruys-Bagger, N., Elmerdahl, J., Praestgaard, E., Tatsumi, H., Spodsberg, N., Borch, K., and Westh, P. (2012) Pre-steady state kinetics for the hydrolysis of insoluble cellulose by *Trichoderma reesei* Cel7A. *J. Biol. Chem.* **287,** 18451–18458
16. Cruys-Bagger, N., Tatsumi, H., Ren, G. R., Borch, K., and Westh, P. (2013) Transient kinetics and rate-limiting steps for the processive cellobiohydrolase Cel7A: effects of substrate structure and carbohydrate binding domain. *Biochemistry* **52,** 8938–8948
17. Igarashi, K., Koivula, A., Wada, M., Kimura, S., Penttilä, M., and Samejima, M. (2009) High speed atomic force microscopy visualizes processive movement of *Trichoderma reesei* cellobiohydrolase I on crystalline cellulose. *J. Biol. Chem.* **284,** 36186–36190
18. Igarashi, K., Uchihashi, T., Koivula, A., Wada, M., Kimura, S., Okamoto, T., Penttilä, M., Ando, T., and Samejima, M. (2011) Traffic jams reduce hydrolytic efficiency of cellulase on cellulose surface. *Science* **333,** 1279–1282
19. Jalak, J., and Väljamäe, P. (2010) Mechanism of initial rapid rate retardation in cellobiohydrolase catalyzed cellulose hydrolysis. *Biotechnol. Bioeng.* **106,** 871–883
20. Kurasin, M., and Väljamäe, P. (2011) Processivity of cellobiohydrolases is limited by the substrate. *J. Biol. Chem.* **286,** 169–177
21. Fox, J. M., Levine, S. E., Clark, D. S., and Blanch, H. W. (2012) Initial- and processive-cut products reveal cellobiohydrolase rate limitations and the role of companion enzymes. *Biochemistry* **51,** 442–452
22. Maurer, S. A., Bedbrook, C. N., and Radke, C. J. (2012) Cellulase adsorption and reactivity on a cellulose surface from flow ellipsometry. *Ind. Eng. Chem. Res.* **51,** 11389–11400
23. Nakamura, A., Watanabe, H., Ishida, T., Uchihashi, T., Wada, M., Ando, T., Igarashi, K., and Samejima, M. (2014) Trade-off between processivity and hydrolytic velocity of cellobiohydrolases at the surface of crystalline cellulose. *J. Am. Chem. Soc.* **136,** 4584–4592
24. Shang, B. Z., Chang, R., and Chu, J. W. (2013) Systems-level modeling with molecular resolution elucidates the rate-limiting mechanisms of cellulose decomposition by cellobiohydrolases. *J. Biol. Chem.* **288,** 29081–29089
25. Zakariassen, H., Eijsink, V. G. H., and Sorlie, M. (2010) Signatures of activation parameters reveal substrate-dependent rate determining steps in polysaccharide turnover by a family 18 chitinase. *Carbohydr. Polym.* **81,** 14–20
26. Cruys-Bagger, N., Elmerdahl, J., Praestgaard, E., Borch, K., and Westh, P. (2013) A steady-state theory for processive cellulases. *FEBS J.* **280,** 3952–3961
27. Praestgaard, E., Elmerdahl, J., Murphy, L., Nymand, S., McFarland, K. C., Borch, K., and Westh, P. (2011) A kinetic model for the burst phase of processive cellulases. *FEBS J.* **278,** 1547–1560
28. Laidler, K. J., and Peterman, B. F. (1979) Temperature effects in enzyme kinetics. *Methods Enzymol.* **63,** 234–257
29. Lonhienne, T., Gerday, C., and Feller, G. (2000) Psychrophilic enzymes: revisiting the thermodynamic parameters of activation may explain local flexibility. *Biochim. Biophys. Acta* **1543,** 1–10

30. Marx, J. C., Collins, T., D'Amico, S., Feller, G., and Gerday, C. (2007) Cold-adapted enzymes from marine antarctic microorganisms. *Mar. Biotechnol.* **9,** 293–304

31. Alasepp, K., Borch, K., Cruys-Bagger, N., Badino, S., Jensen, K., Sørensen, T. H., Windahl, M. S., and Westh, P. (2014) *In situ* stability of substrate-associated cellulases studied by DSC. *Langmuir* **30,** 7134–7142

32. Cruys-Bagger, N., Ren, G., Tatsumi, H., Baumann, M. J., Spodsberg, N., Andersen, H. D., Gorton, L., Borch, K., and Westh, P. (2012) An amperometric enzyme biosensor for real-time measurements of cellobiohydrolase activity on insoluble cellulose. *Biotechnol. Bioeng.* **109,** 3199–3204

33. Horn, S. J., Sørlie, M., Vårum, K. M., Väljamäe, P., and Eijsink, V. G. (2012) Measuring processivity. *Methods Enzymol.* **510,** 69–95

34. Medve, J., Karlsson, J., Lee, D., and Tjerneld, F. (1998) Hydrolysis of microcrystalline cellulose by cellobiohydrolase I and endoglucanase II from *Trichoderma reesei*: adsorption, sugar production pattern, and synergism of the enzymes. *Biotechnol. Bioeng.* **59,** 621–634

35. von Ossowski, I., Ståhlberg, J., Koivula, A., Piens, K., Becker, D., Boer, H., Harle, R., Harris, M., Divne, C., Mahdi, S., Zhao, Y., Driguez, H., Claeyssens, M., Sinnott, M. L., and Teeri, T. T. (2003) Engineering the exo-loop of *Trichoderma reesei* cellobiohydrolase, Ce17A. A comparison with *Phanerochaete chrysosporium* Cel7D. *J. Mol. Biol.* **333,** 817–829

36. Wilson, D. B. (2012) Processive and nonprocessive cellulases for biofuel production-lessons from bacterial genomes and structural analysis. *Appl. Microbiol. Biotechnol.* **93,** 497–502

37. Jalak, J., Kurašin, M., Teugjas, H., and Väljamäe, P. (2012) Endo-exo synergism in cellulose hydrolysis revisited. *J. Biol. Chem.* **287,** 28802–28815

38. Kipper, K., Väljamäe, P., and Johansson, G. (2005) Processive action of cellobiohydrolase Cel7A from *Trichoderma reesei* is revealed as 'burst' kinetics on fluorescent polymeric model substrates. *Biochem. J.* **385,** 527–535

39. Kostylev, M., Alahuhta, M., Chen, M., Brunecky, R., Himmel, M. E., Lunin, V. V., Brady, J., and Wilson, D. B. (2014) Cel48A from *Thermobifida fusca*: structure and site directed mutagenesis of key residues. *Biotechnol. Bioeng.* **111,** 664–673

40. Anslyn, E. V., and Dougherty, D. A. (2004) *Modern Physical Organic Chemistry*, University Science Books, Sausalito, CA

41. Alsallaq, R., and Zhou, H. X. (2007) Energy landscape and transition state of protein-protein association. *Biophys. J.* **92,** 1486–1502

42. Vijayakumar, M., Wong, K. Y., Schreiber, G., Fersht, A. R., Szabo, A., and Zhou, H. X. (1998) Electrostatic enhancement of diffusion-controlled protein-protein association: comparison of theory and experiment on barnase and barstar. *J. Mol. Biol.* **278,** 1015–1024

43. Pu, J., Gao, J., and Truhlar, D. G. (2006) Multidimensional tunneling, recrossing, and the transmission coefficient for enzymatic reactions. *Chem. Rev.* **106,** 3140–3169

44. Johnson, K. A. (1992) in *The Enzymes* (Sigman, D. S., ed) pp. 1–61, Academic Press, San Diego, CA

45. Jalak, J., and Väljamäe, P. (2014) Multi-mode binding of cellobiohydrolase Cel7A from *Trichoderma reesei* to cellulose. *PLoS One* **9,** e108181

46. Medve, J., Ståhlberg, J., and Tjerneld, F. (1997) Isotherms for adsorption of cellobiohydrolase I and II from *Trichoderma reesei* on microcrystalline cellulose. *Appl. Biochem. Biotechnol.* **66,** 39–56

47. Igarashi, K., Wada, M., Hori, R., and Samejima, M. (2006) Surface density of cellobiohydrolase on crystalline celluloses—a critical parameter to evaluate enzymatic kinetics at a solid-liquid interface. *FEBS J.* **273,** 2869–2878

48. Ståhlberg, J., Johansson, G., and Pettersson, G. (1991) A new model for enzymatic hydrolysis of cellulose based on the two-domain structure of cellobiohydrolase I. *Nat. Biotechnol.* **9,** 286–290

49. Colussi, F., Sørensen, T. H., Alasepp, K., Kari, J., Cruys-Bagger, N., Windahl, M. S., Olsen, J. P., Borch, K., and Westh, P. (2015) Probing substrate interactions in the active tunnel of a catalytically deficient cellobiohydrolase (Cel7). *J. Biol. Chem.* **290,** 2444–2454

50. Murphy, L., Borch, K., McFarland, K. C., Bohlin, C., and Westh, P. (2010) A calorimetric assay for enzymatic saccharification of biomass. *Enzyme Microb. Technol.* **46,** 141–146

51. Tewari, Y. B., Lang, B. E., Decker, S. R., and Goldberg, R. N. (2008) Thermodynamics of the hydrolysis reactions of 1,4-β-D-xylobiose, 1,4-β-D-xylotriose, D-cellobiose, and D-maltose. *J. Chem. Thermodyn.* **40,** 1517–1526

52. Page, M. I., and Jencks, W. P. (1971) Entropic contributions to rate accelerations in enzymic and intramolecular reactions and the chelate effect. *Proc. Natl. Acad. Sci. U.S.A.* **68,** 1678–1683

53. Amzel, L. M. (1997) Loss of translational entropy in binding, folding, and catalysis. *Proteins Struct. Funct. Genet.* **28,** 144–149

54. Gilson, M. K., Given, J. A., Bush, B. L., and McCammon, J. A. (1997) The statistical-thermodynamic basis for computation of binding affinities: a critical review. *Biophys. J.* **72,** 1047–1069

55. Tamura, A., and Privalov, P. L. (1997) The entropy cost of protein association. *J. Mol. Biol.* **273,** 1048–1060

56. Murphy, K. P., Xie, D., Thompson, K. S., Amzel, L. M., and Freire, E. (1994) Entropy in biological binding processes— estimation of translational entropy loss. *Proteins Struct. Funct. Genet.* **18,** 63–67

57. Divne, C., Ståhlberg, J., Teeri, T. T., and Jones, T. A. (1998) High-resolution crystal structures reveal how a cellulose chain is bound in the 50 Å long tunnel of cellobiohydrolase I from *Trichoderma reesei*. *J. Mol. Biol.* **275,** 309–325

58. Taylor, C. B., Payne, C. M., Himmel, M. E., Crowley, M. F., McCabe, C., and Beckham, G. T. (2013) Binding site dynamics and aromatic-carbohydrate interactions in processive and non-processive family 7 glycoside hydrolases. *J. Phys. Chem. B* **117,** 4924–4933

59. Beckham, G. T., Matthews, J. F., Peters, B., Bomble, Y. J., Himmel, M. E., and Crowley, M. F. (2011) Molecular-level origins of biomass recalcitrance: decrystallization free energies for four common cellulose polymorphs. *J. Phys. Chem. B* **115,** 4118–4127

60. Bu, L., Beckham, G. T., Shirts, M. R., Nimlos, M. R., Adney, W. S., Himmel, M. E., and Crowley, M. F. (2011) Probing carbohydrate product expulsion from a processive cellulase with multiple absolute binding free energy methods. *J. Biol. Chem.* **286,** 18161–18169

61. Kari, J., Olsen, J., Borch, K., Cruys-Bagger, N., Jensen, K., and Westh, P. (2014) Kinetics of cellobiohydrolase (Cel7A) variants with lowered substrate affinity. *J. Biol. Chem.* **289,** 32459–32468

62. Tailford, L. E., Offen, W. A., Smith, N. L., Dumon, C., Morland, C., Gratien, J., Heck, M. P., Stick, R. V., Blériot, Y., Vasella, A., Gilbert, H. J., and Davies, G. J. (2008) Structural and biochemical evidence for a boat-like transition state in β-mannosidases. *Nat. Chem. Biol.* **4,** 306–312

63. Wicki, J., Williams, S. J., and Withers, S. G. (2007) Transition-state mimicry by glycosidase inhibitors: a critical kinetic analysis. *J. Am. Chem. Soc.* **129,** 4530–4531

64. Yamamoto, K. (1974) A quantitative approach to the evaluation of 2-acetamide substituent effects on the hydrolysis by Taka-N-acetyl-β-D-glucosaminidase. Role of the substrate 2-acetamide group in the N-acyl specificity of the enzyme. *J. Biochem.* **76,** 385–390

65. Sinnott, M. L. (1990) Catalytic mechanisms of enzymatic glycosyl transfer. *Chem. Rev.* **90,** 1171–1202

66. Weber, J. P., and Fink, A. L. (1980) Temperature-dependent change in the rate-limiting step of β-glucosidase catalysis. *J. Biol. Chem.* **255,** 9030–9032

67. Payne, C. M., Resch, M. G., Chen, L., Crowley, M. F., Himmel, M. E., Taylor, L. E., 2nd, Sandgren, M., Ståhlberg, J., Stals, I., Tan, Z., and Beckham, G. T. (2013) Glycosylated linkers in multimodular lignocellulose-degrading enzymes dynamically bind to cellulose. *Proc. Natl. Acad. Sci. U.S.A.* **110,** 14646–14651

68. Adney, W. S., Jeoh, T., Beckham, G. T., Chou, Y.-C., Baker, J. O., Michener, W., Brunecky, R., and Himmel, M. E. (2009) Probing the role of N-linked glycans in the stability and activity of fungal cellobiohydrolases by mutational analysis. *Cellulose* **16,** 699–709

69. Jeoh, T., Michener, W., Himmel, M. E., Decker, S. R., and Adney, W. S. (2008) Implications of cellobiohydrolase glycosylation for use in biomass conversion. *Biotechnol. Biofuels* **1,** 10

70. Palonen, H., Tenkanen, M., and Linder, M. (1999) Dynamic interaction of *Trichoderma reesei* cellobiohydrolases Cel6A and Cel7A and cellulose at equilibrium and during hydrolysis. *Appl. Environ. Microbiol.* **65,** 5229–5233

71. Sørensen, T. H., Cruys-Bagger, N., Windahl, M. S., Badino, S. F., Borch, K., and Westh, P. (2015) Temperature effects on kinetic parameters and substrate affinity of Cel7A cellobiohydrolases. *J. Biol. Chem.* **290,** 22193–22202